Title: An Adaptive Semi-Supervised Approach to the Detection of User-Defined Recurrent Changes in Image Time Series

Author(s): D. Capella Zanotta, L. Bruzzone, F. Bovolo, Y.E. Shimabukuro

AN ADAPTIVE SEMI-SUPERVISED APPROACH TO THE DETECTION OF USER-DEFINED RECURRENT CHANGES IN IMAGE TIME SERIES

Daniel C. Zanotta, *Student Member,* Lorenzo Bruzzone, *Fellow*, *IEEE*, Francesca Bovolo, *Senior Member*, *IEEE*, Yosio E. Shimabukuro

Abstract – **In this paper we present a novel domain adaptation technique aimed at providing reliable change detection maps for series of image pairs acquired on the same area at different times. The proposed technique exploits the polar change vector analysis method and assumes that reference data for characterizing a specific change of interest are available only for a pair of images (source domain). Then it exploits the knowledge learned from the source domain and adapts it to other pairs of images belonging to the time series (target domains) to be analyzed. The proposed technique is able to handle possible radiometric differences among images adapting in an unsupervised way the decision rule estimated on the source domain to the target domains through variables estimated directly on the target images. The proposed approach has been applied to two data sets made up of time series of Landsat Thematic Mapper images. In one case the change of interest is related to evolution of deforestation, while in the other case it is related to burned areas detection. Experimental results show the effectiveness of the proposed technique.**

Index Terms – Recurrent change, domain adaptation, change detection, time series, deforestation, forest fires.

I. INTRODUCTION

The availability of image time series (sequence of images taken from the same area at different times) has driven the interest of the scientific community toward the development of effective methods for the automatic extraction of information from this kind of data. Image time series are especially valuable for detecting changes and/or sequentially updating land-cover maps [1-4]. This

1

kind of information is highly important to improve environmental monitoring and support decision makers. In this context, an interesting application is the one related to the identification of changes which tend to occur systematically on the ground. These kinds of changes are due to recurrent phenomena like deforestation, fires, floods, etc. that periodically affect the Earth.

These applications are nowadays mainly faced by using standard change detection methods [5],[6]. Traditional approaches implicitly treat every new image pair in the time series as a new change-detection problem. However, when dealing with recurrent changes, the target change is the same for each pair of images and thus it is expected to show similar behaviors, although not identical, to those observed in previously analyzed image pairs. In other words, recurrent changes generate similar, yet slightly different, effects in different couples of images within the time series. Possible differences may arise from noisy components such as radiometric differences due to seasonal effects or atmospheric conditions, sub-optimal co-registration, etc. [7],[8].

In this context, the decision rule defined to detect a specific kind of change in a given pair of images cannot be used on other image pairs in the time series as it is. However, it is reasonable to take advantage of similarities and adapt the decision rule in an effective way to determine the parameters for each new pair of images. The concept of adaptation in remote sensing image analysis has been already investigated in the remote sensing literature for classification problems. As an example, transfer learning techniques have been recently proposed aimed to perform domain adaptation between domains in supervised classification problems [9]-[13]. These techniques are often understood as semi-supervised learning methods that exploits the information on a given image (source domain) to obtain effective results on another image as they are able to use only spatially or temporally limited information (target domains) [13]. To best reach this goal, it is often assumed that the target land cover classes are the same in the source and target domains, and that classes follow similar statistical distribution even if characterized by different parameter values [7],[14]. Despite domain adaptation techniques can be found in the literature for the classification of

multitemporal images [14],[15], only few methods [8],[16] can be found assuming that changes might have occurred between acquisitions. However, none of them deals with adaptation in the context of change detection.

An extensive survey of change detection methods in remote sensing images is out the scope of this paper. The reader is referred to [17]-[24] for further literature analysis. Here we focus our attention on the use of optical images acquired by passive sensors and one of the most common unsupervised change detection approaches for such images: the polar Change Vector Analysis (CVA) [25]. CVA computes Spectral Change Vectors (SCVs) by subtracting two multitemporal multispectral images pixel by pixel and performs the analysis of SCVs for change information extraction. SCVs can be expressed in hyperspherical coordinates according to their magnitude and a set of direction variables [26]. However, often for the sake of simplicity and visualization purposes, CVA is performed in a 2-dimensional space by considering only 2 spectral channels (or relevant features). Accordingly, only the magnitude and one direction variable are used for modeling change information. The magnitude contains information about the presence/absence of changes [1], [26], whereas direction variable(s) carries information about the kind of change [27]. Each kind of change is expected to show a preferred direction which is usually different from those of the others [28]. The preferred direction is determined by the spectral properties of each specific kind of change.

In this paper, we propose to take advantage of the properties of changes in the SCV feature space in order to properly characterize recurrent changes in multiple pairs of multitemporal images based on the expectation that recurrent changes show similar preferred direction(s) independently on the considered image pair. To this end, we propose an adaptive semi-supervised approach to the detection of single recurrent changes in image time series. The proposed approach takes advantage of the repetitive nature of recurrent changes to adapt the change detection decision rule computed for a given pair of multitemporal images (source domain) to a new multitemporal pair of images

(target domain) expected to show the same kind of change, i.e., to show a similar scenario. The method is based on three concepts: (i) a 3-dimensional (3D) representation of SCVs; (ii) the definition of a decision rule that optimizes the detection of the change of interest in the source domain; and (iii) the adaptation of the above-mentioned decision rule to the target domain for the automatic detection of the recurrent kind of change in new upcoming image pairs.

The rest of the paper is organized into five sections. The next section formulates the problem and gives an overview of the proposed method. Section III introduces the approach to model the change information in a 3D spherical coordinate system. The representation is valid for both source and target domains. Section IV presents the proposed adaptation technique for detection of recurrent changes in image time series. Section V illustrates the experimental results obtained on a time series of TM-Landsat image acquired over an area in Brazil where deforestation and forest fires are recurrently destroying vegetation. Finally, Section VI draws the conclusion of this work.

II. BACKGROUND AND PROBLEM FORMULATION

Let us consider a time series $TS = \{\mathbf{X}_1, \mathbf{X}_2, \ldots, \mathbf{X}_Q\}$ made up of Q co-registered and radiometrically corrected multitemporal images acquired over the same geographical area at times $1, \ldots, Q$, respectively. Each $\mathbf{X}_q$ ($q = 1, \ldots, Q$) can be represented by the image spectral channels and/or any possible kind of feature derived from them. Let N be the total number of elements composing each of the considered images. An element here may be either a single pixel or an object derived according to a segmentation process [29]. Let $\Omega = \{\omega_{nc}, \omega_{rc}, \omega_{ic}\}$ be the set of classes to be detected, where ω_{nc} is the class of non-changed elements, ω_{rc} is the change class relevant for the considered application, and ω_{ic} is the class grouping all other possible kinds of change (*i.e.*, the ones irrelevant to the considered application). In our formulation, ω_{ic} shows a small occurrence with respect to the recurrent relevant kind of change. Let us assume, without any loss of general validity, that a reliable ground truth (GT) is available and models the recurrent change of relevance (ω_{rc})

4

occurred on the ground between the source domain multitemporal pair $\mathbf{X}_1$ and $\mathbf{X}_2$. GT can be entire or partially available for the area covered by the images, provided that it properly models the change of relevance. If no GT is available, it is reasonable to expect that the user can easily define a reliable ground truth map for at least one pair of images to be used for initializing the adaptation process. Each image pair in *TS* with available multitemporal ground truth information can be used as source domain pair without any loss of validity. All other image pairs different from the source domain are the target domain image pairs.

The proposed method first computes the multidimensional difference image $\mathbf{X}_D$ for the source domain according to (1):

$$\mathbf{X}_D = \mathbf{X}_2 - \mathbf{X}_1. \tag{1}$$

$\mathbf{X}_D$ and the available ground truth information are used to derive in a supervised way a decision region (R) for the recurrent change of interest ω_{rc} in the source domain. Once the decision region R for ω_{rc} is known in the source domain, the detection of ω_{rc} in the target domain (*i.e.*, in each possible pair of images in TS) requires the adaptation of R to the properties of the target image pair. To this end, a multispectral difference image $\mathbf{X}_D^t$ is computed for the target pair and a new decision region R^t is estimated by adapting R to $\mathbf{X}_D^t$ for each considered target domain data set. Fig. 1 shows the block scheme of the proposed approach. In Fig 1, E_p^* is an optimal set of elementary regions which supports the definition of R.
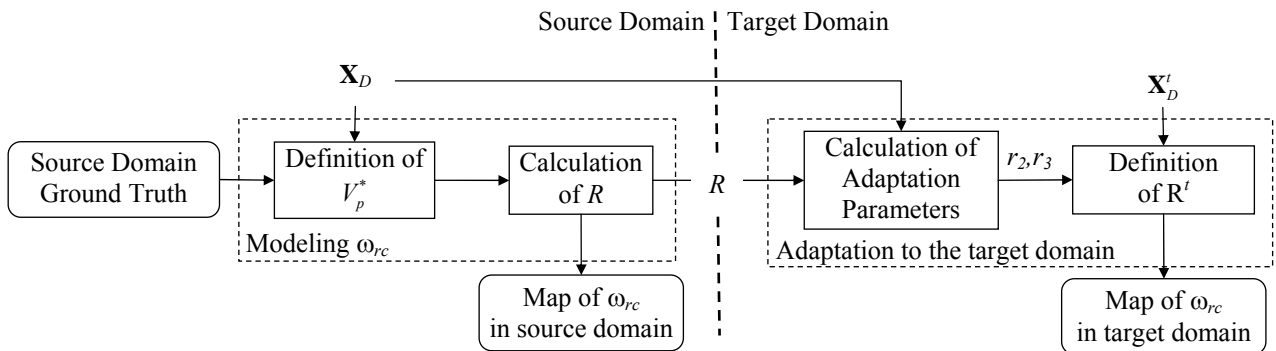

Fig. 1. Block diagram of the proposed approach.

III. 3-DIMENSIONAL REPRESENTATION OF CHANGE INFORMATION

In this section we first extend the 2D Change Vector Analysis given in [27] to the use in a 3D feature space and illustrate how the properties of spectral change vectors $\mathbf{X}_D(n)$ ($n=1,\ldots, N$) are employed to define the decision region R that properly models the relevant recurrent change ω_{rc} in the source domain. Let us consider 3 features (*i.e.*, $M = 3$), being either the original spectral channels or features extracted from them (*e.g.*, vegetation indices or texture features). Under this assumption, each element in $\mathbf{X}_D$ can be represented in spherical coordinates according to its magnitude (ρ), azimuth angle (θ) and elevation angle (φ). The relationship between Cartesian coordinates represented by the $\mathbf{X}_D$ features and spherical coordinates is given by:

$$
\begin{cases}
\rho = \sqrt{X_{D,1}^2 + X_{D,2}^2 + X_{D,3}^2} \\[2mm]
\theta = \arctan\left(\dfrac{X_{D,2}}{X_{D,1}} \right) \\[2mm]
\varphi = \arccos\left(\dfrac{X_{D,3}}{\rho} \right)
\end{cases}
\tag{2}
$$

where $X_{D,1}$, $X_{D,2}$ and $X_{D,3}$ represent the Cartesian coordinates of spectral change vectors in $\mathbf{X}_D$, while $\rho \in [0, +\infty[$ is the magnitude, $\theta \in [0, 2\pi[$ is azimuth angle, and $\varphi \in [0, \pi[$ is the elevation angle. Fig. 2 depicts the relation between the two coordinate systems for a generic SCV.
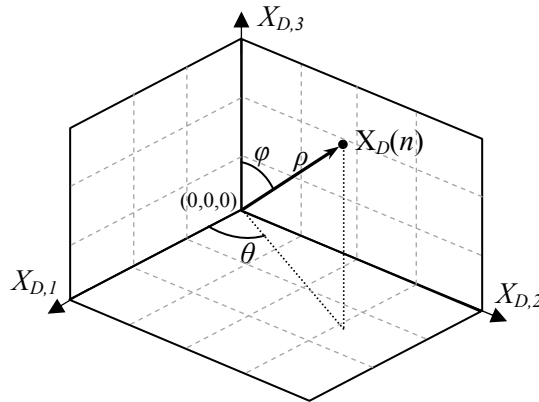

Fig. 2. Spatial correspondence between Cartesian and spherical coordinates systems.

In spherical coordinates, the domain of existence of all SCVs in $\mathbf{X}_D$ (Figure 3a) is defined as:

$$S = \left\{ \rho, \varphi, \theta : \ 0 \le \rho < \rho_{max}, \ 0 \le \varphi < 2\pi, \ 0 \le \theta < \pi \right\}, \tag{3}$$

where ρ_{max} is the largest magnitude value among the elements in $\mathbf{X}_D$

$$\rho_{max} = \max_{n=1,\ldots,N} \left\{ \sqrt{X_{D,1}^2(n) + X_{D,2}^2(n) + X_{D,3}^2(n)} \right\}. \tag{4}$$

As known from the literature [25],[27] the value of the magnitude ρ of SCV carries information about the presence/absence of changes, whereas the direction variables carry information about the kind of change.

According to this observation, and following [26], sub-regions of relevance are identified in S (Figure 3a). A first sub-region S_{nc} is associated to unchanged elements. These elements are expected to assume small magnitude values along directions [27]. This is considered to be independent of the dimensionality of the spherical space, given that images are radiometrically corrected. Therefore they are expected to cluster within a sphere concentric to S. The S_{nc} sphere is defined as

$$S_{nc} = \left\{ \rho, \varphi, \theta : \ 0 \le \rho < \rho_T, \ 0 \le \varphi < 2\pi, \ 0 \le \theta < \pi \right\}, \tag{5}$$

where ρ_T is a threshold separating the unchanged (near the origin) from the changed elements (far from the origin) along the magnitude variable. S_{nc} is depicted as the small gray sphere in Figure 3b.

The region S_c complementary to S_{nc} with respect to S is defined as

$$S_c = \left\{ \rho, \varphi, \theta : \ \rho_T \le \rho < \rho_{max}, \ 0 \le \varphi < 2\pi, \ 0 \le \theta < \pi \right\}. \tag{6}$$

S_c is characterized by high magnitude values and includes elements of all kinds of change. Inside this volume, changed elements cluster along a specific direction (θ_k, φ_k) depending on the kind of change (Figure 3c). The regions in S_c including each kind of change can be represented by a solid angle which is geometrically modeled as a truncated cone R with square basis. The cone has the vertex in the origin of S and two spherical bases. The major base lays on the external surface of S and the minor one on the external surface of S_{nc}. Geometrically speaking, the cone is a 3-
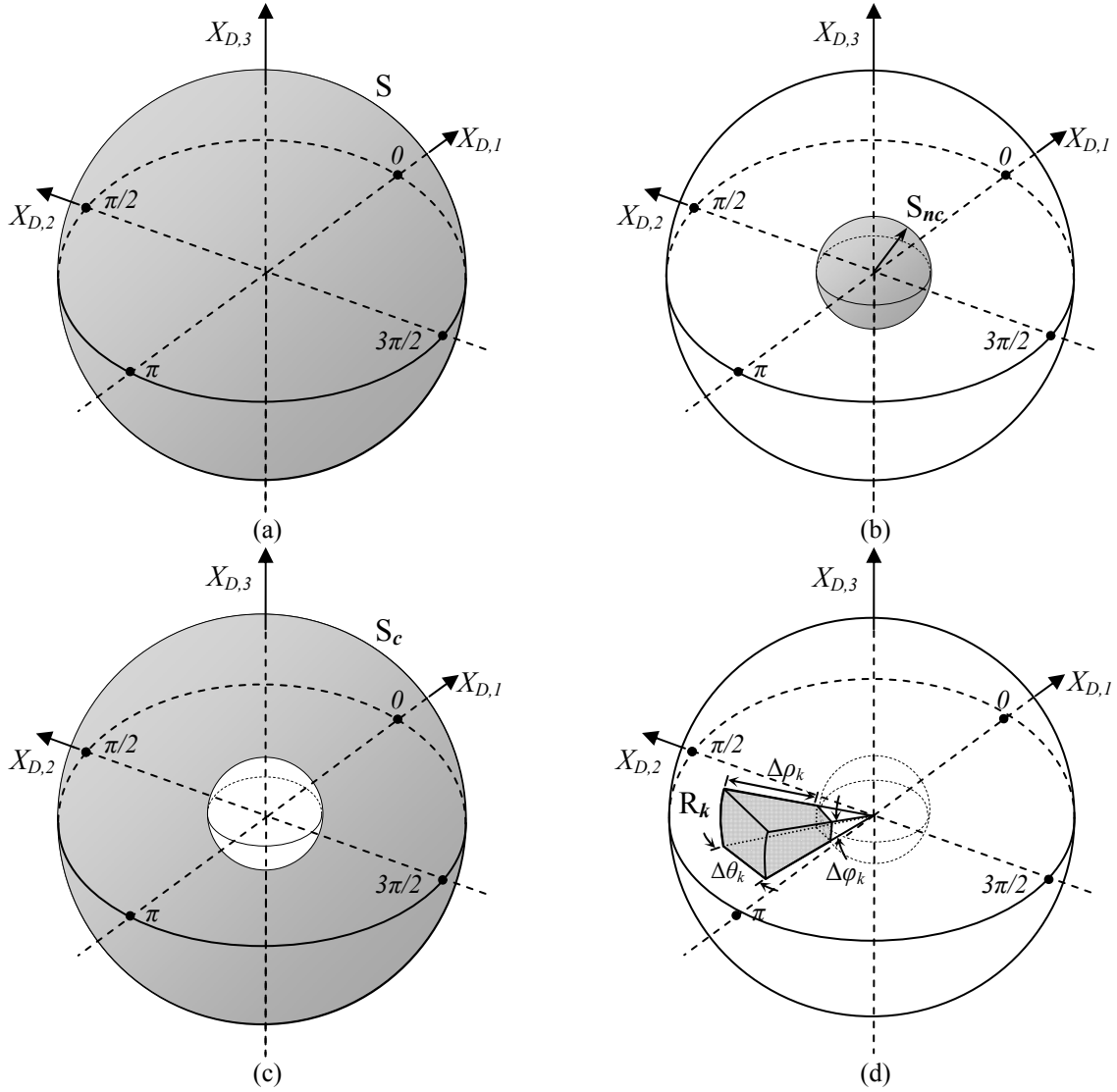
Fig.3. Regions of interest for the CVA technique in spherical coordinates: (a) domain *S* of existence of all SCVs in X_D, (b) sphere S_{nc} of no-changed elements, (c) spherical shell S_c including changed elements, and (d) solid truncated cone R_k associated to a generic change *k*.

dimensional shape which tapers smoothly from a flat base (usually, but not necessarily, circular) to a point called vertex [30]. The rationale for choosing this solid lays on the ability to properly model the slight variations in θ and φ along different magnitude values ρ. The region R_k associated to a generic change *k* (either relevant or irrelevant) is defined as

$$R_k = \left\{ \rho, \varphi, \theta: \ \rho_T \leq \rho < \rho_{\max}, \ \varphi_{k_1} \leq \varphi < \varphi_{k_2}, \ \theta_{k_1} \leq \theta < \theta_{k_2} \right\} \tag{7}$$

whe

8

re $\varphi_{k_1}, \varphi_{k_2}, \theta_{k_1}, \theta_{k_2}$ identify the upper and lower bound along elevation and azimuth variables, respectively. For each R_k, the ranges along the magnitude $\Delta\rho_k = \rho_{max} - \rho_T$, the azimuth $\Delta\theta_k = \theta_{k_2} - \theta_{k_1}$, and the elevation $\Delta\varphi_k = \varphi_{k_2} - \varphi_{k_1}$ is defined as depicted in Figure 3d.

The illustrated framework is general and can be used to detect multiple kinds of change in the 3D feature space, *i.e.* to solve change detection problems showing an arbitrary number K of changes. However, in this work we consider that only one single change is mostly affecting the area of interest; this is the relevant recurrent change ω_{rc}. Therefore, in the following we consider only one truncated cone needs to be identified in the source domain R and adapted to obtain the truncated cone R^t in the target domain(s) by an unsupervised technique. Accordingly, in the following the subscript k is omitted to simplify the notation and ease readability. Thus, R represents the decision region associated to the recurrent change ω_{rc} and is fully described by its upper and lower bounds along the magnitude, azimuth and elevation: $\rho_{max}, \rho_T, \theta_2, \theta_1, \varphi_2$ and φ_1, respectively. The specific direction along which changed elements cluster becomes (θ_R, φ_R).

IV. MODELLING OF THE RECURRENT CHANGE IN THE SOURCE DOMAIN

In this section, the procedure for selecting the optimal decision region R for the detection of the recurrent changes of relevance in the source domain is presented.

As mentioned above, changed patterns show statistical behavior significantly different from the unchanged ones and they cluster along a specific direction (θ_R, φ_R). Therefore, it is expected that data maximum variance occurs along the direction (θ_R, φ_R) after filtering unchanged elements. Accordingly, it is reasonable to expect that the directions of the first and second eigenvectors derived from Principal Component Analysis (PCA) applied to $\mathbf{X}_D$ (in the Cartesian feature space) are naturally associated with the dispersion of the recurrent change ω_{rc}. In this work we apply the methodology in [1] to obtain, in an unsupervised way, the threshold value ρ_T (*i.e.*, the radius of

sphere S_{nc}), that separates changed from unchanged elements (Fig. 3b). Following [1], the Expectation Maximization (EM) algorithm can be used to estimate statistical parameters (*i.e.*, mean and variance) of change and unchanged patterns along ρ variable. As done in [1] the statistical distribution of both classes is modeled as Gaussian. Once the parameters are set (here EM algorithm is used for parameter estimation, initialized by taking advantage of the ground truth information), a Bayesian decision rule is applied to identify unchanged elements and remove them from the analysis. Therefore, only elements within S_c. (i.e., the ones with high magnitude value) remain. The new dataset without unchanged elements is named here as $\mathbf{X}_{Df}$ and includes by definition all the elements such that $\mathbf{X}_D(n) \in S_c$. Given the expected similarity between source and target domains, the initial EM values for the target domain are extended to the source domain. In order to identify the region R associated with ω_{rc} the proposed method quantizes S_c in a set of elementary volumes V_p ($p=1, \ldots, N_V$) with pre-defined 3D size $\Delta\theta_V$, $\Delta\varphi_V$ and $\Delta\rho_V$. For a specific change detection problem, the total number of elementary volumes (N_V) necessary to cover S_c depends on the pre-defined size of V_p, as well as on the values of ρ_T and $\rho_{\max}$. The number N_V is computed as

$$N_V = \frac{2\pi^2(\rho_{\max} - \rho_T)}{\Delta\theta_V \Delta\varphi_V \Delta\rho_V}.$$ (8)

It is worth noting that the size of V_p must be chosen in order to result in an integer number N_V. Each elementary volume V_p is a subset of S_c, and S_c can be expressed as the union of all V_p as

$$S_c = \bigcup_{p=1}^{N_V} V_p.$$ (9)

In order to properly characterize the relevant recurrent change ω_{rc} in the source domain taking advantage of the 3-dimensional CVA framework, V_p should be identified that contains a high number of ω_{rc} elements. To this end, we use the available GT information by selecting only V_p having correct detections larger than false alarms by applying the following rule:

$$\frac{\left|X_D(V_p) \in \omega_{rc}\right|}{\left|X_D(V_p) \in \{\omega_{rc} \cup \omega_{nc}\}\right|} > 0.5 \qquad p \in [1, N_V], \ n = 1, ..., N, \tag{10}$$

where |.| returns the cardinality of the corresponding set. 0.5 ensures an acceptable trade-off between the selection of volumes V_p properly capturing the specific characteristics of ω_{rc}. The goal is to exclude regions containing few correct detections and the avoid a too restrictive characterization resulting in poor performance of the next adaptation to the target domain(s) step. In addition, this threshold allows one to take into account possible outliers in the reference map. The threshold value 0.5 can be changed according to the user needs. The selected set of volumes V_p^* might not be spatially adjacent in S_c, but they are expected to distribute along a preferred direction. A qualitative representation of the set of volumes V_p^* and their relation to R is depicted in Fig. 4. The subset of the elements of $\mathbf{X}_{Df}$ included in the identified V_p^* is defined as

$$\mathbf{X}_D^* = \bigcup_{p=1}^{N_V} \mathbf{X}_{Df}(V_p^*). \tag{11}$$

The elements in $\mathbf{X}_D^*$ are used to define the position of the region R describing the behaviors of ω_{rc}.
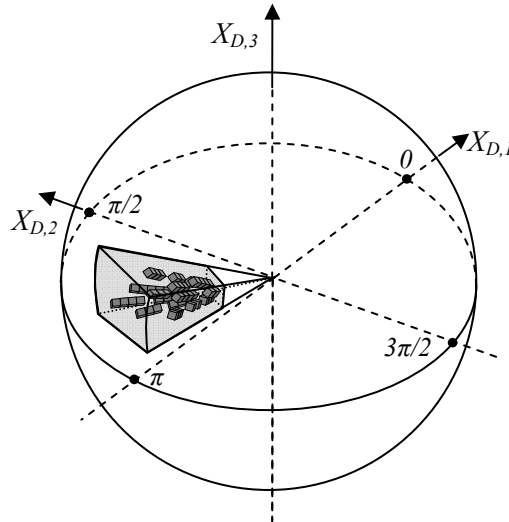

Fig. 4. Representation of V_p volumes (dark gray shaded volumes) and their relation to R (light gray shaded volume).

11

The procedure for defining R exploits the dispersion of $\mathbf{X}_D^*$ to approximate the size and direction of R in a vector basis and does not make any assumption on their statistical model. It only considers that the elements of ω_{rc} are clustered along a preferred direction. Therefore PCA is applied only to $\mathbf{X}_D^*$. According to PC properties, the 1st eigenvector of $\mathbf{X}_D^*(\upsilon_1^*)$ is associated with the main direction of ω_{rc} (*i.e.*, the direction of the maximum dispersion). Thus, υ_1^* approximates the direction of axis of the cone R and is expressed in azimuth and elevation coordinates as:

$$\begin{cases} \theta_R \equiv \theta_{\upsilon_1} = \arctan\left(\dfrac{\upsilon_{1,2}^*}{\upsilon_{1,1}^*} \right) \\ \varphi_R \equiv \varphi_{\upsilon_1} = \arccos\left(\upsilon_{1,3}^* \right) \end{cases}, \tag{12}$$

where θ_{υ_1}, φ_{υ_1} are the spherical coordinates of the first eigenvector, $\upsilon_{1,1}$, $\upsilon_{1,2}$ and $\upsilon_{1,3}$ are the three components of the 1st eigenvector computed with $\mathbf{X}_D^*$ in the Cartesian feature space.

Since PC's are orthogonal to each other, the second and third PC's are used to quantify the 2-dimensional dispersion of $\mathbf{X}_D^*$ around the axis of R (Fig. 4a) orthogonal to the maximum dispersion one. In other words, the angular dimension of R defined by $\Delta\varphi_R$ and $\Delta\theta_R$ is modeled based on the 2nd and 3rd eigenvalues λ_2^* and λ_3^* of $\mathbf{X}_D^*$. The two R small edges are estimated with respect of these last eigenvalues as λ_2^* and λ_3^* (Fig. 5). For convenience, R edges were approximate as linear in their angles computation. According to the scheme of Fig. 5b and 5c, the aperture angles $\Delta\varphi_R$ and $\Delta\theta_R$ are written by means of ρ_T, λ_2^*, λ_3^* and basic trigonometric relations:

$$\begin{cases} \Delta\varphi_R = 2 \cdot \arctan\left(\dfrac{\lambda_2^*}{2\rho_T} \right) \\ \Delta\theta_R = 2 \cdot \arctan\left(\dfrac{\lambda_3^*}{2\rho_T} \right) \end{cases}, \tag{13}$$

Accordingly the complete 3D boundaries of R are defined as:

$$\begin{cases} \theta_1 = \dfrac{\Delta\varphi_R}{2} - \theta_R \\[2mm] \varphi_1 = \dfrac{\Delta\theta_R}{2} - \varphi_R \\[2mm] \rho_1 = \rho_T \end{cases} \quad \text{and} \quad \begin{cases} \theta_2 = \dfrac{\Delta\varphi_R}{2} + \theta_R \\[2mm] \varphi_2 = \dfrac{\Delta\theta_R}{2} + \varphi_R, \\[2mm] \rho_2 = \rho_{max} \end{cases} \tag{14}$$

The labeling of elements $\mathbf{X}_D$, resulting in the change detection map $\mathbf{M}$ of the recurrent change, is obtained by applying the following decision rule:

$$\mathbf{M}(n) \in \begin{cases} \omega_{rc} & \text{if } X_D(n) \in R \\ \omega_{ic} \cup \omega_{nc} & \text{otherwise} \end{cases} \quad \forall n \in [1, N]. \tag{15}$$
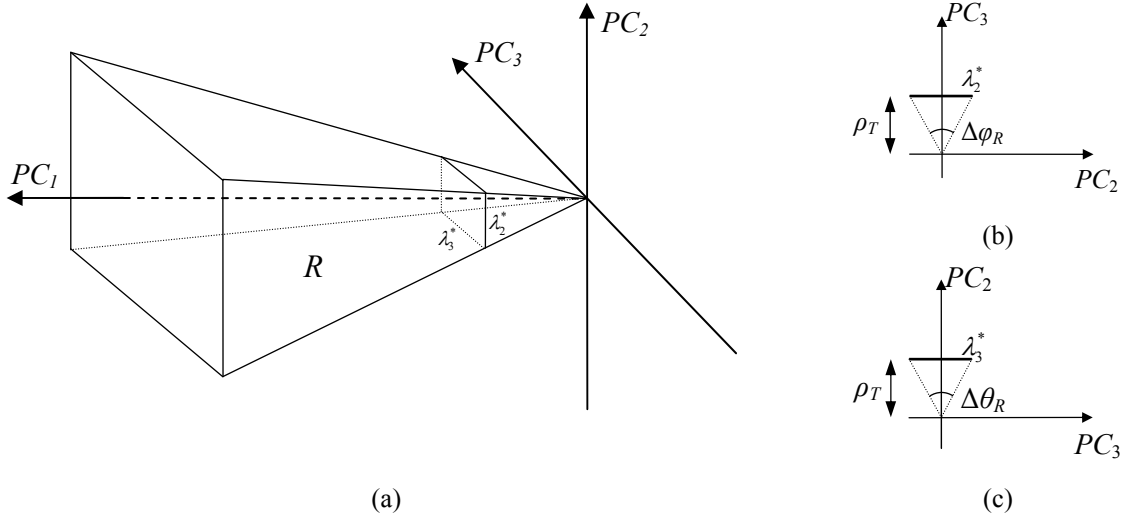

(a)

(b)

(c)

Fig. 5. Scheme related to the estimation of the decision region R in the PC feature space computed for $X^*_D(n)$: (a) spatial representation of the decision region R, (b) diagram for estimation of φ_R from λ^*_2, and (c) diagram for estimation of θ_R from λ^*_3.

Despite R is a decision region that detects the recurrent change of relevance with a given margin in the source domain, when applied to the target domain it is expected to result in poor performance. As mentioned in Sec. I, this is due to the fact that a recurrent change may show small differences in the statistical behavior (and thus direction and dispersion in S_c) because of several factors not strictly related to the kind of change itself and despite radiometric corrections have been applied. Therefore, depending on the domain-to-domain variations of the change of interest, the size and direction of R may need to be adapted. The next step of the proposed methodology aims to

13

drive the adaptation of the previously defined region R, which was defined by using GT, to a new realization of the same kind of change when no reference data are available for the considered pair of images (target domain).

V. ADAPTATION OF THE CHANGE DETECTION DECISION RULE TO THE TARGET DOMAIN

The adaptation strategy involves the adjustment of R parameters θ_R, φ_R, ρ_T, $\Delta\rho_R$, $\Delta\theta_R$, $\Delta\varphi_R$ to the properties of ω_{rc} in the target domain. Let $\mathbf{X}_D^t$ be the difference image computed by applying (1) in the target domain, and let S_c^t be the region associated to changed elements in the target domain. S_c^t computed in an unsupervised way by following the same procedure described for the source domain. S_c^t satisfies the definition (6) in the target domain. The updating of R, which results in R^t, starts by defining the main direction of R^t. This parameter is computed as the direction of the 1st eigenvector υ_1^t associated to the elements $\mathbf{X}_{Df}^t$ ($\mathbf{X}_{Df}^t$ corresponds to $\mathbf{X}_D^t$ without unchanged elements). It is important to note that, as no GT is available to target domains, the main direction of R^t is computed on $\mathbf{X}_{Df}^t$, instead of $\mathbf{X}_D^{*t}$. This is reasonable since we are working with only one relevant change occurred and S_c^t mostly contains this relevant change. Therefore, it is expected that the ratio between the second and third eigenvalues for elements in S_c and V_p^*, respectively, computed in the source domains is preserved for the same quantities in the target domain(s). This observation is used to estimate the real dispersion presented by the elements of recurrent change in the target domain, updating the size of R. Thus, the coefficients of adaptation is obtained by following ratios:

$$r_2 = \frac{\lambda_2^*}{\lambda_2^f}, \qquad r_3 = \frac{\lambda_3^*}{\lambda_3^f}, \qquad (16)$$

where r_2 and r_3 refer to the proportionality between the second and third dispersions of patterns in $\mathbf{X}_{Df}$ and $\mathbf{X}_D^*$ for the source domain, λ_2^* and λ_3^* are eigenvalues for $\mathbf{X}_D^*$ and λ_2^f and λ_3^f are

14

eigenvalues for $\mathbf{X}_{Df}$. A point to be highlighted is the independency of the eigenvalues from the number of patterns. This ensures that, even though the amount of patterns associated with the considered specific change increases or decreases in the target domain the coefficients of adaptation can still be effectively applied. By now, we empirically assume that the adaptation coefficients r_2 and r_3 being stable over a given time-series.

At this point we can estimate eigenvalues related to the patterns standing for the change of relevance in the target domain λ_2^{*t} and λ_3^{*t}, which are the edges of the cone R^t adapted to the target domain(s) by using coefficients r_2 and r_3, and eigenvalues λ_2^t and λ_3^t computed on S_c^t:

$$\begin{cases} \lambda_2^{*t} = \lambda_2^t \cdot r_2 \\ \lambda_3^{*t} = \lambda_3^t \cdot r_3 \end{cases}.$$ (17)

Equation (17) exploits knowledge about the specific change of relevance in the source domain through coefficients r_2 and r_3. These estimations are based on the established relationship between the whole spread of the data after removing the unchanged patterns and the one related only to the patterns of the specific change made in Equation (15). The aperture angles $\Delta\varphi_{R^t}$, $\Delta\theta_{R^t}$ as well as, the spatial limits of R^t is computed in a similar manner to that used to define R with the equations (13) and (14). The decision region R^t for the change of interest is finally defined as

$$R^t = \left\{ \rho, \varphi, \theta : \ \rho_T^t \leq \rho < \rho_{\max}^t, \ \varphi_1^t \leq \varphi < \varphi_2^t, \ \theta_1^t \leq \theta < \theta_2^t \right\},$$ (18)

and the generalized decision rule resulting in the change detection map $\mathbf{M}^t$ of the recurrent change in the target domain becomes:

$$\mathbf{M}^t(n) \in \begin{cases} \omega_{rc} & if \ X_D^t(n) \in R^t \\ \omega_{ic} \cup \omega_{nc} & otherwise \end{cases} \quad \forall n \in [1, N].$$ (19)

The steps performed to define R^t as defined in (19) need to be recomputed for every new pair of images representing the target domain.

VI. EXPERIMENTS AND RESULTS

A. Data Set Description and Design of Experiments

The proposed methodology has been tested on two multitemporal data sets made up of time series acquired by the Thematic Mapper (TM) multispectral sensor onboard of Landsat-5 satellite. The first data set refers to a 1500×1500 pixels subset showing many deforestation activities in Brazilian Amazon. This is the main kind of change observed at regular intervals of time on the study area and occurs as small fragments of deforestation. The official methodology adopted to detect deforestation in the Brazilian Amazon region at spatial resolution of 30m is PRODES. PRODES is mainly based on photointerpretation carried out by experts [35]. The reason for using this approach is the difficulty to find a single method effective for every scenario. Other systems such as DETER and FORMA are also used for mapping deforestation, but they do not represent a meaningful comparison since they provide results at a lower spatial resolution (250 m and 1000 m, respectively). The time series used in this experiment is made up of five co-registered multispectral images acquired each September (dry season) from 2006 to 2011. A false color composition of the images is shown in Fig. 6. As PRODES is based on an object oriented visual interpretation, in order to maintain the same referential of analysis, we segmented the images and used the regions as elements. Segmentation obtained on the second image (target domain) in the multitemporal pair is applied to the first image (source domain) as well. The resulting elements are used to compute attributes for both images, avoiding misalignment among objects. The three attributes selected for the Amazon data set were: i) TM channel 5 (0.85-0.88μm), ii) NDVI computed from TM channels 3 (0.53-0.59μm) and 4 (0.64-0.67μm), and iii) the entropy of the first PC derived from channels 3, 4 and 5, which models the texture. These attributes were defined taking into account the properties of change of interest: deforestation. The first image pair (2007-2008) was used as the source domain and the remaining ones (2008-2009, 2009-2010, 2010-2011) as target domains. To avoid double detection, in each pair, the previously detected deforestation were masked, and removed from the

16

subsequent pair analysis (*i.e.*, there cannot be again deforestation on the same area over a short period). In this data set, instrumental and atmospheric variations, and short scale wheatear conditions just before image acquisitions (which may strongly affect vegetation) cause radiometric differences among the images.

September/2007   September/2008   September/2009
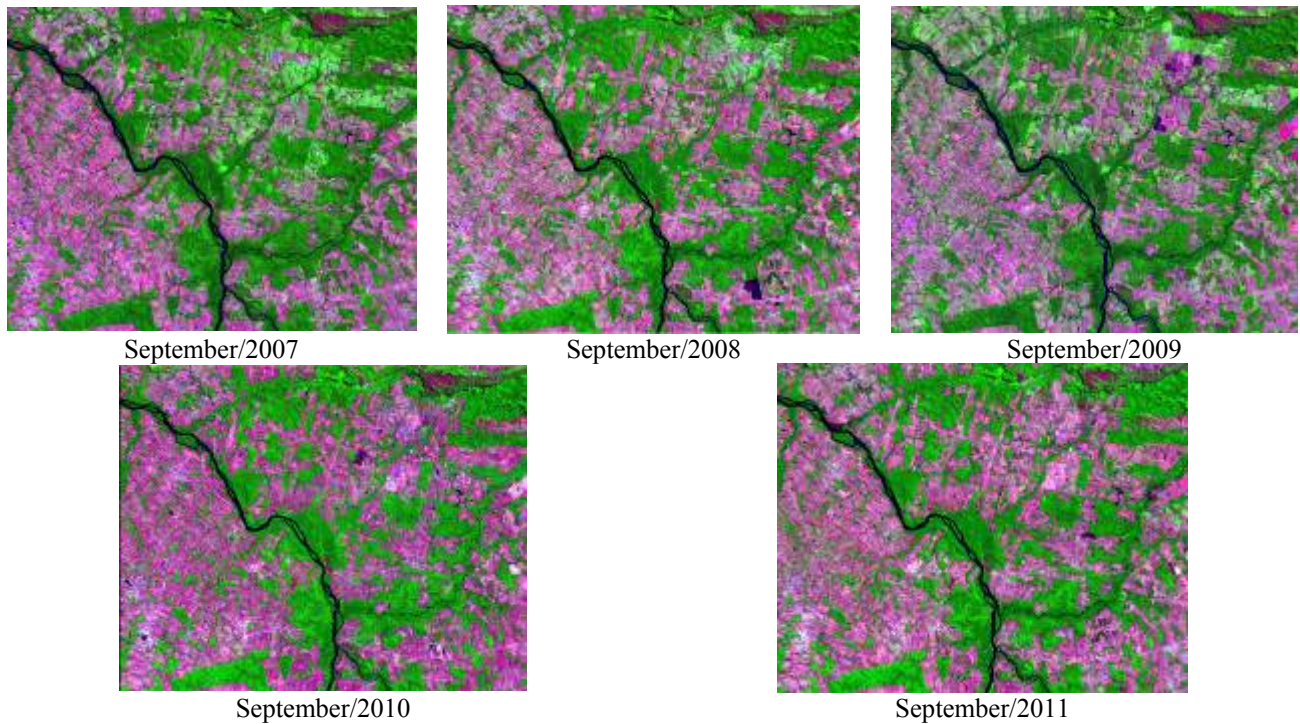
September/2010   September/2011

Fig. 6. False color composition of images in the multitemporal TM-Landsat-5 image time series (2007-2011) used for the Amazon data set [5(R), 4(G), 3(B)]. Magenta color highlights bare soil areas and areas associated to deforestation processes.

The second data set refers to a 500×500 pixels area of the Brazilian Pantanal marked by several recursive fires. The data set is made up by three co-registered images acquired in May 2006, July 2006 and July 2007. Among the acquisitions, no additional land-cover classes were observed, but burned areas. False color composites of the images are shown in Fig. 7. For the Pantanal data set we used the channels 3, 4 and 5 as input features. SWIR Landsat channel 5 is known to be efficient for burned areas detection. As for the first data set, we considered the two first images as source domain, whereas the second and third images were considered as target domain. Unlike the forested Amazon environment, the vegetation present at Pantanal is shallow and sparse, and thus is affected by strong variations. Natural vegetation variations occur on the ground in addition to the application

17

relevant change which is associated to effects of forest fires, thus the experiment becomes highly challenging.

| May/2006 | July/2006 | July/2007 |

Fig. 7. False color composition Multitemporal TM-Landsat-5 image time series used in the Pantanal data set [5(R), 4(G), 3(B)]. Dark brown highlights bare soil area due to fire events.

For both data sets, radiometric normalization was performed by atmospheric correction of the individual images in the time series. In addition, by considering that the amount of changes is smaller than the amount of unchanged elements, a further normalization was made by subtracting from the t_1 images the mean value computed for its corresponding difference image. Thus the mean value for each feature of the difference image resulted to be zero. GT was built for each subsequent pair of images. The one of the source domain is required for applying the proposed method. The ones for target domains are used only for accuracy assessment and are not involved in the adaptation process which is performed in a semi-supervised fashion. The R^t estimated for the target domains by automatic domain adaptation were compared with the best possible R^t computed in a supervised way according to available GT. For the first data set only, the results were compared to PRODES data concerning the same area and acquisition date. In the following subsections, we present the experimental details and the results obtained on the considered data sets.

B. Results for Deforestation in Amazon Rainforest

After segmentation and attribute extraction on single date images, feature extraction in the source domain is carried out at region level. Fig. 8a depicts the scatterplot in spherical coordinates

of the attributes of the source domain multitemporal difference image $\mathbf{X}_D$. According to the proposed approach the threshold ρ_T is computed in the source domain which is equal to 8.3. The suppression of elements with magnitude lower than ρ_T was performed resulting in $\mathbf{X}_{Df}$ (see Fig. 8b). The resulting S_c was subdivided into E_p. In the following, results are reported by using $\Delta\theta=\Delta\varphi=5^{\circ}$, $\Delta\rho=5$. However, results demonstrated to be stable with $\Delta\theta$ and $\Delta\varphi$ in $]0,5]$, which is a reasonable wide range if considering the spread of ω_{rc} along θ and φ, respectively. The algorithm is less sensitive to the value of $\Delta\rho$. It is worth noting that the selection of small values may result in a significant increase of the computational time. The steps leading to the definition of elementary volumes E_p having correct detections larger than false alarm rate (Fig. 8c) were computed. The selection of elements inside the set of elementary volumes V_p^* was derived according to (11), resulting in the elements $\mathbf{X}_D^*$ depicted in Fig. 8d. The next step involves the definition of R for the source domain by applying PCA to $\mathbf{X}_{Df}$ and $\mathbf{X}_D^*$. Fig. 8b and 8d show the directions of the three PCs computed for $\mathbf{X}_{Df}$ and $\mathbf{X}_D^*$, which have a large similarity in terms of directions of the PCs. This fact corroborates our assumption on the correlation between $\mathbf{X}_{Df}$ and $\mathbf{X}_D^*$ dispersion. The direction of the first eigenvector of $\mathbf{X}_{Df}$ is the estimated main direction of R. The size $\Delta\varphi_R$ and $\Delta\theta_R$ of R is predicted by applying (13) and (14). We finally have the conditions to define the generalized decision rule for the source domain, which is based on the size and direction of R.

The next step is the adaptation of R to the target domain(s). First unchanged patterns are identified and removed by estimating ρ_T^t on ρ^t according to [1]. Resulting scatterplots of $\mathbf{X}_{Df}^t$ for each target domain are shown in Fig. 9. Adaptation parameters r_2 and r_3 are computed with support of reference data in the source domain through (16) and the size and direction of R^t is defined for each target domain. In Table 1 the magnitude thresholds ρ_T^t as well as the angular size of R^t computed for each target domain are summarized.
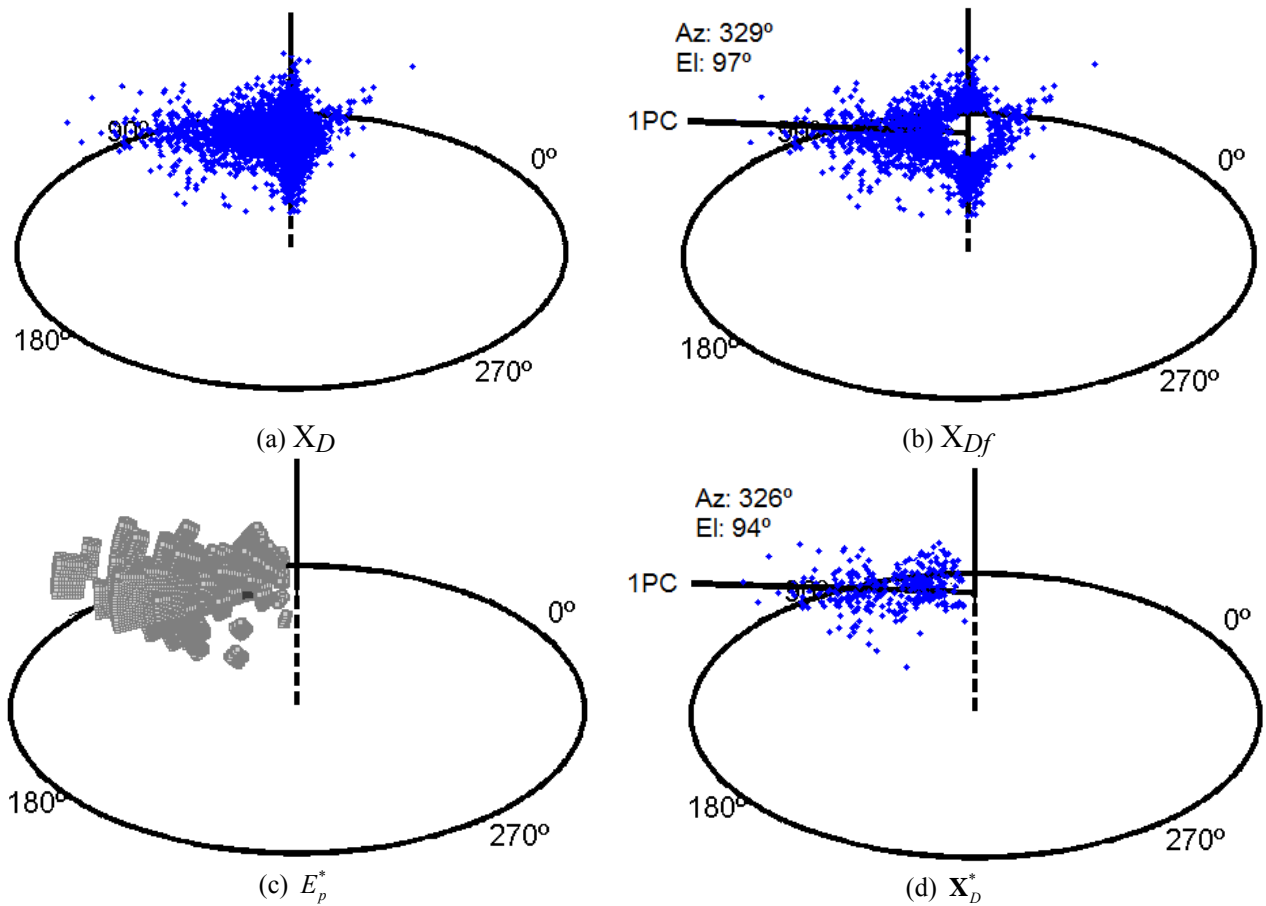
19

Fig. 8. Scatterplot of (a) X_D, (b) X_Df, (c) optimal regions E_p^* computed with GT support, and (d), patterns in $\mathbf{X}_D^*$. The black lines in (b) and (d) are first PC (1PC) direction for the respective scatterplot. (Amazon Data Set).

Due to the small size of deforestation fragments, a visual analysis of the resulting change maps is not enough to have a reliable validation of the method. The results were thus analyzed in terms of number of correct detections and false alarm rates (see Table 2). Table 2 also compares the results obtained with the proposed methodology to those achieved by PRODES for the same area and periods. The proposed methodology shows largely improved detection rates when compared to PRODES. The same improvement was observed for false alarm rates; with the only exception of the 2009-2010 image pair (see Table 2). For 2008-2009, both PRODES and the proposed method reached poor results compared to the other scenarios. This can be explained by the large amount of forest fires occurred during this period (easily noticeable in the images of Fig. 6). In such a situation the working hypothesis that only one kind of change is prevailing, is not fully satisfied. Thus the proposed method is penalized. However, despite the critical situation, the proposed method

achieves in a partially supervised and fast way performance comparable to the ones achieved by PRODES in a time consuming a non-automatic manner. Thus the proposed method resulted to be a valuable tool. It is important to note that, due to variations inherent to PRODES, some of the false alarms in a year are related to missed alarms in the previous period. Thus, the cumulative amount of deforestation estimated in the time series is expected to be accurate, despite possible accuracy variations in the years in which it was detected.
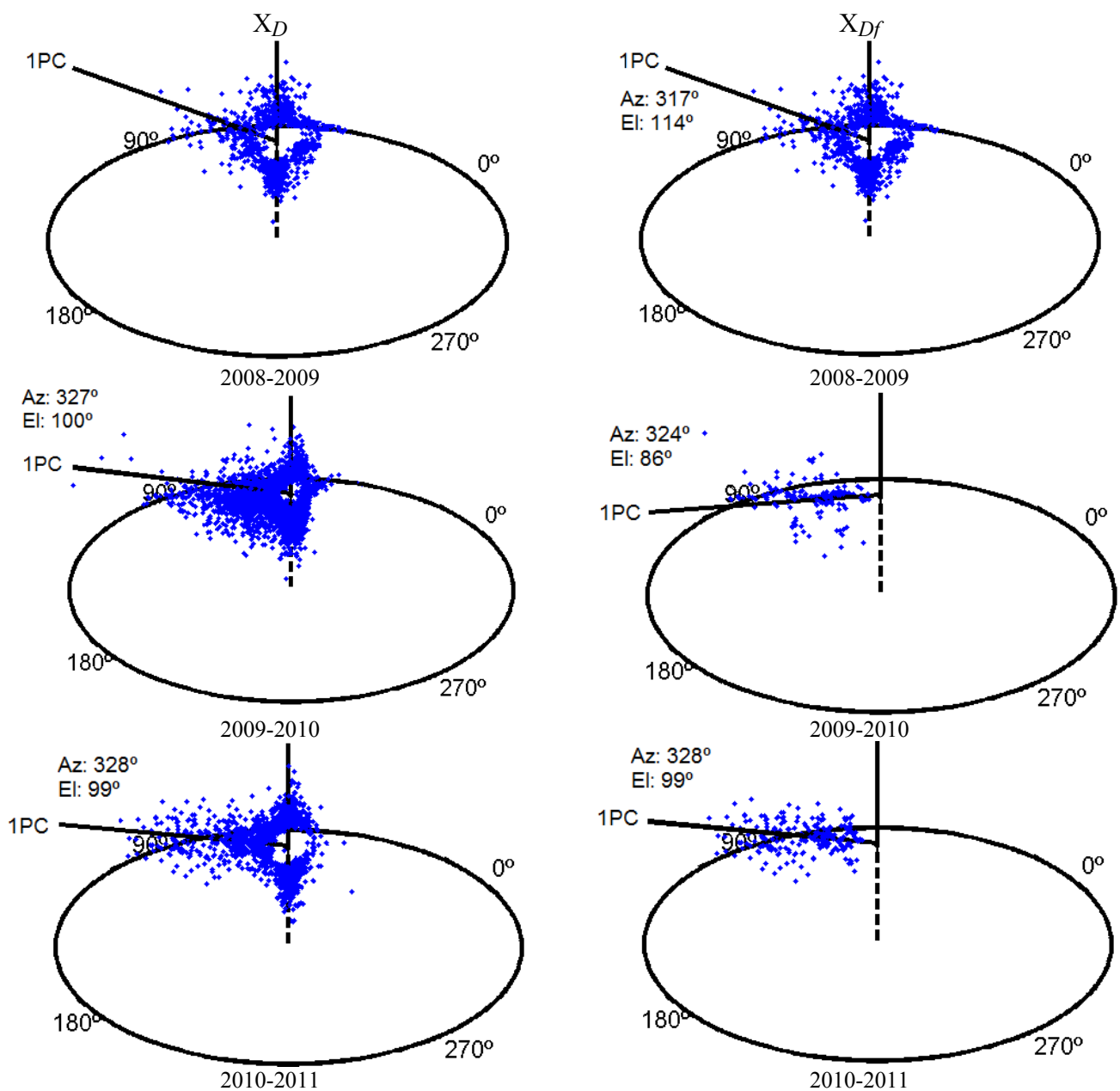

Fig. 9. First column scatterplots depicting X_{Df}^{t*}, Second column, scatter plots depicting X_{D}^{t*} when analyzing each image pair according to the GT. The black lines in the scatterplots are the first PC (1PC) direction. (Amazon Data Set).

21

TABLE 1. COMPUTED $\mathbf{R}^t$ PARAMETERS FOR THE TARGET DOMAIN (AMAZON DATA SET).

Period	ρ_T^t	φ_R^t	θ_R^t
2008-2009	10.8	140º	82º
2009-2010	7.0	144º	55º
2010-2011	10.0	140º	36º

TABLE 2. ACCURACY (%) IN TERMS OF DETECTED CHANGES AND FALSE ALARMS (DETECTED / FALSE), (AMAZON DATA SET).

Technique	2007-2008	2008-2009	2009-2010	2010-2011
PRODES	56 / 56	43 / 64	32 / 43	41 / 50
Proposed Methodology	67 / 39	45 / 37	72 / 62	77 / 31

C. Experimental Results for Fires in Pantanal

In order to further validate the proposed method a second data set was considered. The same steps as for the first data set were applied. The change of interest is in this case related to areas affected by fires, which are expected to show negative values for channels 2 and 3 in the difference image $\mathbf{X}_D$. Thus the positive values for channels 2 and 3 present in the difference image $\mathbf{X}_D$ (Fig. 10a) were neglected. This choice was made in order to avoid the influence of other kinds of change related to natural vegetation variations, which are not the focus of our analysis for this data set. The result of this pre-processing and of the removal of elements with magnitude smaller than $\rho_T = 13$ is $\mathbf{X}_{Df}$ (Fig. 10b). As for the Amazon data set, the size of each V_p was chosen as $\Delta\theta=\Delta\varphi=5^{\circ}$, $\Delta\rho=5$ (also in this case results resulted to be stable for $\Delta\theta$ and $\Delta\varphi$ in]0,5] and a wide range of $\Delta\rho$). The set of V_p^* elementary volumes resulting for this experiment is shown in Fig. 10c, while $\mathbf{X}_D^*$ is shown in Fig. 10d. From the main direction and size of R based on $\mathbf{X}_D^*$, the adaptation parameters r_2 and r_3 are computed and R^t for the target domain is estimated. The similarity between the directions of the first PCs in Fig. 11a and Fig. 11b indicates the soundness of the proposed approach for the estimation of the main direction of R^t. The magnitude threshold ρ_T^t as well as the angular dimension of R^t computed for each target domain are summarized in Table 3. In Fig. 12b and Fig. 12d show the fire change maps for both the source domain images (computed with R) and the target domain images (computed with R^t). The accuracy assessment points out a 91.5% of correct

detections and 7.5% of false alarms on the source domain, and the proposed method resulted in

93.4% correct change detections and 14.1% false alarms on the target domain (Table 3).

TABLE 3. ACCURACY (%) IN TERMS OF DETECTED CHANGES AND FALSE ALARMS (DETECTED / FALSE), (PANTANAL DATA SET).

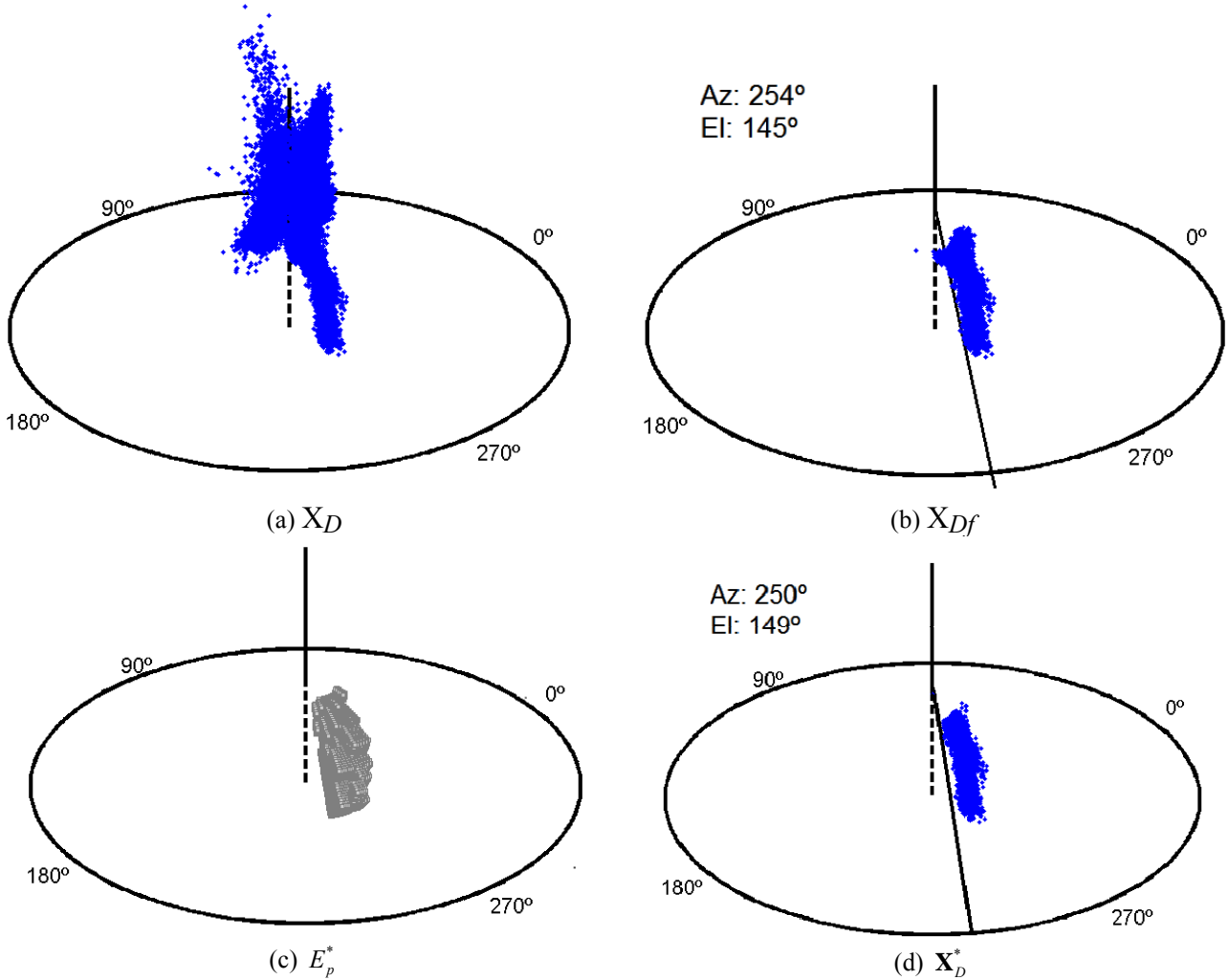| Technique	May/2006-July/2006	July/2006-July/2007
Proposed Methodology	91.5 / 7.5	93.4 / 14.1

Fig. 10. Scatterplots depicting (a) X_D, (b) X_{Df} after suppression of positive values for channels 2 and 3, (c) optimal regions V_p^* computed with GT support, and (d), patterns X_D^*. The black lines in (b) and (d) represents the first PC (1PC) direction for the respective scatterplots. (Pantanal data set).

TABLE 4. COMPUTED R^T PARAMETERS FOR THE TARGET DOMAIN (PANTANAL DATA SET).

Period	ρ_T^t	φ_R^t	θ_R^t
May/2006 - July/2006	12	145°	254°
July/2006 - July/2007	20	153°	255°

By analyzing both change maps we can observe that most of the false alarms are concentrated in

well-defined regions. Visual interpretation of the multispectral images shows us some small

changes in these locations due to vegetation variations. Thus, even if these changes are not associated with fires, they are real changes occurred on the ground.
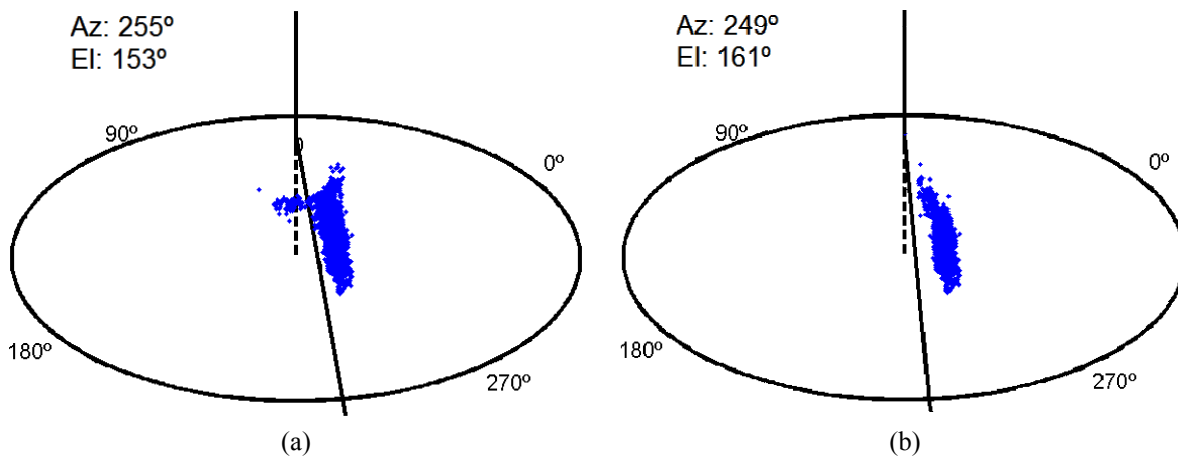

(a)

(b)

Fig. 11. Adaptation results to the target domain and comparison with GT. Scatterplot depicting (a) $\mathbf{X}_{Df}^{t}$, (b) $\mathbf{X}_{D}^{*}$ when analyzing the target domain according to the GT. The black lines in the scatterplots represent the first PC (1PC) direction for the respective data set. (Pantanal data set).

(a)

(b)

24
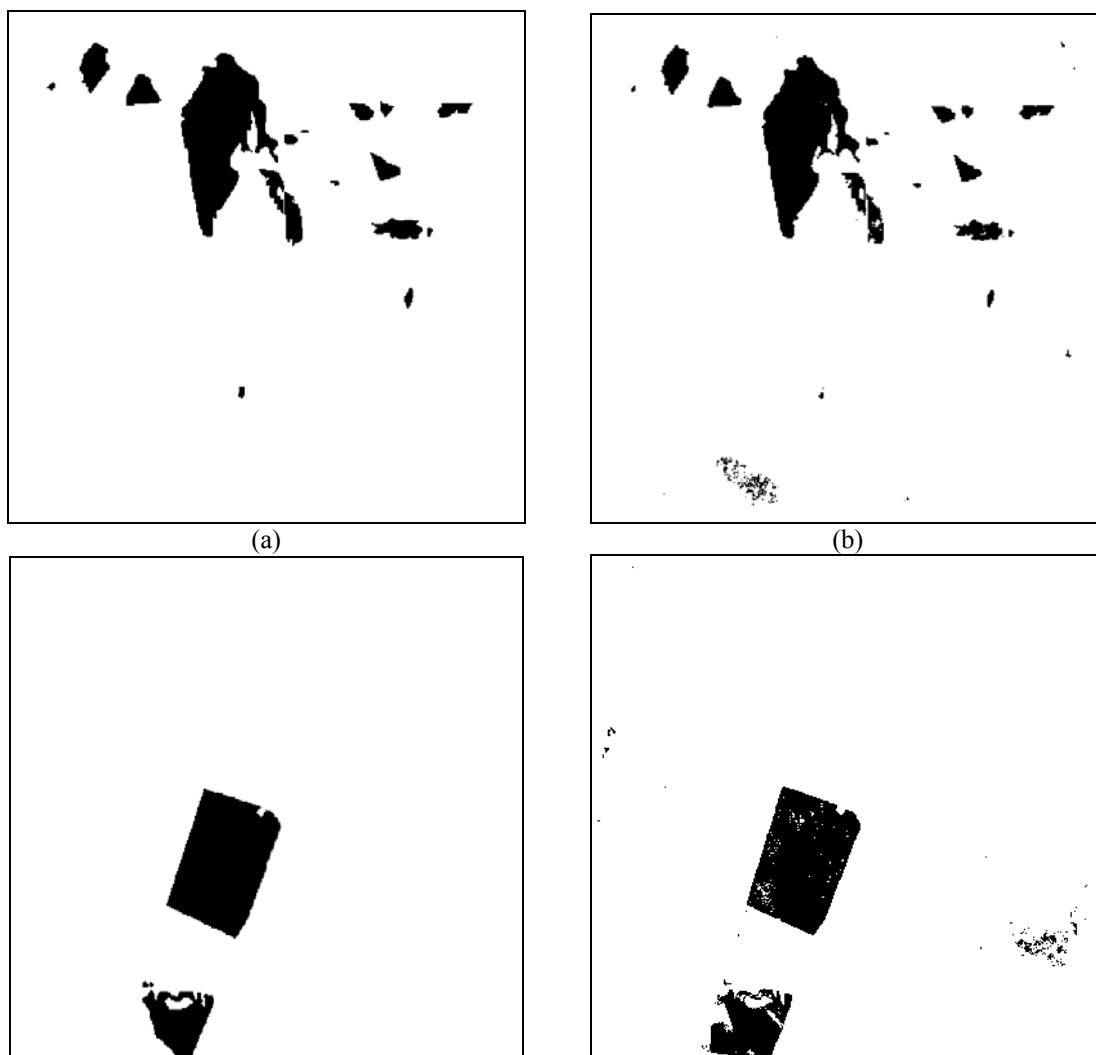
Fig. 12. (a) Reference image for the source domain, (b) change detection maps obtained with the proposed technique, (c) reference image for the target domain, and (d) change detection map obtained with the proposed approach on the target domain. Changes are depicted in black. (Pantanal data set).

VII. CONCLUSIONS

In this paper a novel approach to the detection of recurrent changes in pairs of images extracted from time series has been presented. The proposed approach aims at defining a decision rule supported by reference data available for only one image pair of the time series (source domain), and to adapt it the decision rule to other image pairs (target domains). The method is made up of two steps. The first step selects the most meaningful elementary volumes in a spherical CVA space in order to model the change of interest. These elementary volumes are derived considering a trade-off between correctly detected changes and false alarms according to the reference data GT. At the end of this step, a decision region R is defined for the source domain. The second step is aimed at estimating adaptation parameters in order to extend the solution previously found for the source domain R to other image pairs belonging to the same time series (target domains) R^t. Thus, we obtain an adaptation of the decision regions which is flexible and can be used to recognize the specific change of interest for the whole time series without any additional reference data. This semi-supervised approach represents a valuable tool for many environmental monitoring problems since it requires limited user interaction and information.

Quantitative analysis obtained on two data sets made up of Landsat-5 thematic mapper image time series confirmed the effectiveness of the proposed adaptive technique in detecting specific changes with CVA in spherical coordinates. Unsupervised automatic adaptation compared with results obtained by using reference data for the target domains proved that adaptation results were effective and could be properly used to recognize the change of relevance in other scenarios. Furthermore, results pointed out good capabilities in automatically detecting Amazon deforestation when compared to the time-demanding currently adopted PRODES methodology. It is also important to emphasize that environments with presence of recurrent changes are quite common

and the availability of automatic techniques for updating CD maps in unsupervised way is very important.

As final remarks, it is worth noting that the technique is intended to be applied in stabilized scenarios where the expected changes from time to time are not varying strongly. It is important to note that the technique is designed to only one kind of change. Thus, ensuring the best fitting of the decision rule to the change of relevance in all the involved domains. If there are several kinds of change and they are not stationary among the time series the proposed method may reduce its effectiveness. Moreover, some strategies can be applied to reduce the contribution of changes that may not be of interest. One of them is based on neglecting the portions of the CVA domains that are far from the change of interest (as made here in the second data set). This is done on the basis of the information provided by the prior information on the source domain.

As future developments of this work, we plan to extend the test to other kinds of real applications and large scale environmental problems by also considering the presence of multiple changes of interest. In addition we plan to increase its level of automation.

APPENDIX I

The notation used in the paper is listed in Table 4. It is worth noting that the same variable names has been used for both source and target domains. The table below lists the ones for the source domain. All variables for target domain are obtained by adding a superscript t.

TABLE 4 NOTATION USED IN THE PAPER.

TS = $\{\mathbf{X}_1, \mathbf{X}_2, …, \mathbf{X}_Q\}$	Time series (image spectral channels or features derived from it)
Q	co-registered multispectral images
N	the total number of patterns (pixels/regions)
$\Omega=\{\omega_{nc}, \omega_{rc}, \omega_{ic}\}$	set of classes to be detected
GT	Ground Truth
$\mathbf{X}_D$	difference image for the source domain
$\mathbf{X}_{Df}$	difference image for the source domain after non changed patterns filtering
$\mathbf{X}_D^*$	$\mathbf{X}_D$ elements inside E_p^*
R	decision region of the source domain
$\mathbf{X}_D(n)$	Spectral Change Vector
ρ	magnitude
θ	azimuth angle

φ	elevation angle
S_{nc}	spherical sub-region with unchanged patterns
S_c	sub-region with changed elements
θ_R, φ_R	the main direction of R
ρ_T	magnitude threshold for the source domain
λ_2^f and λ_3^f	eigenvalues for $\mathbf{X}_{Df}$
λ_2^* and λ_3^*	second and third eigenvalues computed for $\mathbf{X}_D^*$
$\rho_{max}, \rho_T, \theta_2, \theta_1, \varphi_2$ and φ_1	upper and lower bound along magnitude, azimuth and elevation variables for R
$\Delta\rho_R, \Delta\theta_R, \Delta\varphi_R$	R ranges
V_p	set of N_V elementary volumes quantizing S_c
$\Delta\theta_V, \Delta\varphi_V$ and $\Delta\rho_V$	size of V_p
V_p^*	selected V_p obeying the best trade-off
$\boldsymbol{\upsilon}_1^*$	first eigenvector for elements in $\mathbf{X}_D^*$
$\boldsymbol{\upsilon}_{1,1}^*, \boldsymbol{\upsilon}_{1,2}^*$ and $\boldsymbol{\upsilon}_{1,3}^*$	three components of the first eigenvector for elements $\mathbf{X}_D^*$
r_2 and r_3	coefficients of adaptation
$\mathbf{M}$	map of recurrent change ω_{rc}

REFERENCES

[1] L. Bruzzone, D. F. Prieto, "Automatic analysis of the difference image for unsupervised change detection," *IEEE Trans. Geosci. Remote Sens*. vol. 38, no. 3, pp. 1171 – 1182, 2000.

[2] D. Lu, P. Mausel, E. Brondizio, E. Moran, "Change detection techniques," *Int. J. Remote Sens.* vol. 25, no. 12, pp. 2365 – 2407, 2003.

[3] L. Castellana, A. D'Addabbo, G. Pasquariello, "A composed supervised/unsupervised approach to improve change detection from remote sensing," *Pattern Recogniton Letters.* vol. 28, no. 4, pp. 405 – 413, 2007.

[4] M. Filippone, G. Sanguinetti, "Information theoretic novelty detection," *Pattern Recognition.* vol. 43, no. 3, pp. 805-814, 2010.

[5] F. G. Hall, D. E. Strebel, J. E. Nickeson, S. J. Goetz, "Radiometric rectification: toward a common radiometric response among multidate, multisensor images," *Remote Sens. Environ.* 35 (1991) 11 – 27.

[6] L. Bruzzone, S. B. Serpico, "An Iterative Technique for the Detection of Land-Cover Transitions in Multitemporal Remote-Sensing Images," *IEEE Trans. Geosci. Remote Sens.* vol. 35, no. 4, pp. 858 – 867, 1997.

[7] B. Demir, F. Bovolo, L. Bruzzone, "Classification of Time Series of Multispectral Images with Limited Training Data," *IEEE Transactions on Image Processing*, vol. 22, pp. 3219-3233. 2013.

[8] B. Demir, F. Bovolo, L. Bruzzone, "Updating land-cover maps by classification of image time series: A novel change-detection-driven transfer learning approach," *IEEE Trans. Geosci. Remote Sens.*, vol. 51, no. 1, pp. 300–312, Jan. 2013.

[9] S. Rajan, J. Ghosh, M. Crawford, "Exploiting class hierarchies for knowledge transfer in hyperspectral data," *IEEE Trans. Geosci. Remote Sens.*, vol. 44, no. 11, pp. 3408–3417, 2006.

[10] L. Bruzzone and M. Marconcini, "Domain adaptation problems: A DASVM classification technique and a circular validation strategy," *IEEE Trans. Pattern Anal. Mach. Intell.*, vol. 32, no. 5, pp. 770–787, 2010.

[11] S. Patra, L. Bruzzone, "A fast cluster-based active learning technique for classification of remote sensing images," *IEEE Trans. Geosci. Remote Sens.*, vol. 49, no. 5, pp. 1617–1626, 2011.

[12] C. Persello, L. Bruzzone, "A novel active learning strategy for domain adaptation in the classification of remote sensing images," in *Proc. IEEE Int. Geosci. Remote Sens. Symp.*, Vancouver, BC, Canada, pp. 3720–3723, 2011.

[13] S. J. Pan, I. W. Tsang, J. T. Kwok, Q. Yang, "Domain adaptation via transfer component analysis," *IEEE Trans. Neural Netw.*, vol. 22, no. 2, pp. 199–210, 2011.

[14] C. Persello, L. Bruzzone, "Active Learning for Domain Adaptation in the Supervised Classification of Remote Sensing Images", *IEEE Transactions on Geoscience and Remote Sensing*, vol. 50, pp. 4468-4483, 2012.

[15] L. Bruzzone, R. Cossu, "A multiple cascade-classifier system for a robust a partially unsupervised updating of land-cover maps", *IEEE Transactions on Geoscience and Remote Sensing*, vol. 40, no. 9, pp. 1984-1996, 2002.

[16] K. Bahirat, F. Bovolo, L. Bruzzone, S. Chaudhuri, "A Novel Domain Adaptation Bayesian Classifier for Updating Land-Cover Maps with Class Differences in Source and Target Domains", *IEEE Transactions on Geoscience and Remote Sensing*, vol. 50, no. 7, pp. 2810-2826, 2012.

[17] P. R. Coppin, I. Jonckheere, K. Nachaerts, "Digital change detection techniques," *Int. J. Remote Sens.*, vol. 25, no. 9, pp. 1565–1596, 2004.

[18] D. Lu, P. Mausel, E. Brondízio, E. Moran, "Change detection techniques," *Int. J. Remote Sens.*, vol. 25, no. 12, pp. 2365–2407, 2004.

[19] A. J. Radke, S. Andra, O. Al-Kofahi, B. Roysam, "Image change detection algorithms: A systematic survey," *IEEE Trans. Image Process.*, vol. 14, no. 3, pp. 294–307, 2005.

[20] F. Pacifici, F. D. Frate, "Automatic change detection in very high resolution images with pulse-coupled neural networks," *IEEE Geosci. Remote Sens. Lett.*, vol. 7, no. 1, pp. 58–62, 2010.

[21] Y. Bazi, F. Melgani, H. D. Al-Sharari, "Unsupervised change detection in multispectral remotely sensed imagery with level set methods," *IEEE Trans. Geosci. Remote Sens.*, vol. 47, no. 8, pp. 3178–3187, 2010.

[22] G. Mercier, G. Moser, S. B. Serpico, "Conditional copulas for change detection in heterogeneous remote sensing images," *IEEE Trans. Geosci. Remote Sens.*, vol. 46, no. 5, pp. 1428–1441, 2008.

[23] D. Faur, C. Vaduva, I. Gavat, M. Datcu, "An information theory based image processing chain for change detection in earth observation," in *Proc. 15th Int. Conf. Syst. Signals Image Process.*, Bratislava, Slovakia, pp. 129–132, 2008.

[24] J. M. Canty, A. A. Nielsen, "Visualization and unsupervised classification of changes in multispectral satellite imagery," *Int. J. Remote Sens.*, vol. 27, no. 18, pp. 3961–3975, 2006.

[25] W. A. Malila, "Change vector analysis: An approach for detecting forest changes with Landsat," in *Proc. LARS Mach. Process. Remotely Sensed Data Symp*. W. Lafayette, IN, pp. 326–336, 1980.

[26] T. Celik, K. K. Ma, "Unsupervised change detection for satellite images using dual-tree complex wavelet transform," *IEEE Trans. Geosci. Remote Sens*, vol. 48, no. 3, pp. 1199-1210, 2010.

[27] F. Bovolo, L. Bruzzone, "A theoretical framework for unsupervised change detection based on change vector analysis in the polar domain," *IEEE Trans. Geosci. Remote Sens,* vol. 45, no. 1, pp. 218-236, 2007.

[28] F. Bovolo, S. Marchesi, L. Bruzzone, "A framework for automatic and unsupervised detection of multiple changes in multitemporal images," *IEEE Trans. Geosci. Remote Sens*, v. 50, n. 6, p. 2196-2212, 2012.

[29] F. Bovolo, "A Multilevel Parcel-Based Approach to Change Detection in Very High Resolution Multitemporal Images", *IEEE Geoscience and Remote Sensing Letters* , vol. 6, no. 1, pp. 33-37, 2009.

[30] G. E. Bredon.. *Topology and Geometry*. Springer-Verlag, NY, 2003.

[31] K. Rank, M. Lendl, R. Unbehauen, "Estimation of image noise variance", In: *Vision, Image and Signal Processing, IEE Proceedings,* vol. 146, no. 2, pp. 80-84, 1999.

[32] B. R. Corner, R. M. Narayanan, S. E. Reichenbach, "Noise estimation in remote sensing imagery using data masking", *International Journal of Remote Sensing*, v. 24, n. 4, pp. 689-702, 2003.

[33] C. Liu, R. Szeliski, S. B. Kang, C. L. Zitnick, W. T. Freeman, "Automatic estimation and removal of noise from a single image", *IEEE Transactions on Pattern Analysis and Machine Intelligence*, vol. 30, no. 2, pp. 299-314, 2008.

[34] S. Sari, H. Roslan, T. Shimamura, "Noise estimation by utilizing mean deviation of smooth region in noisy image", In: *IEEE Fourth International Conference on Computational Intelligence, Modelling and Simulation (CIMSiM),* pp. 232-236, 2012.

[35] INPE, "Amazon Rainforest monitoring by satellites," PRODES, 2003.

[36] G. Câmara, Souza, R. C. M. Souza, U. M. Freitas, J. Garrido, "SPRING: Integrating remote sensing and GIS by object-oriented data modeling," *Computers & graphics*, vol. 20, no. 3, p. 395-403, 1996.